New Journal of Physics
The open access journal at the forefront of physics

Deutsche Physikalische Gesellschaft DPG IOP Institute of Physics

FAST TRACK COMMUNICATION • OPEN ACCESS

Skyrmion production on demand by homogeneous DC currents

To cite this article: Karin Everschor-Sitte *et al* 2017 *New J. Phys.* **19** 092001

View the article online for updates and enhancements.

You may also like

- Skyrmions and Hall transport
Bom Soo Kim
- Topological aspects of antiferromagnets
V Bonbien, Fengjun Zhuo, A Salimath et al.
- Transcription and logic operations of magnetic skyrmions in bilayer cross structures
Kai Yu Mak, Jing Xia, Xichao Zhang et al.

This content was downloaded from IP address 87.154.141.141 on 13/09/2022 at 17:52

New Journal of Physics
The open access journal at the forefront of physics

Deutsche Physikalische Gesellschaft DPG
IOP Institute of Physics

Published in partnership with: Deutsche Physikalische Gesellschaft and the Institute of Physics

OPEN ACCESS

RECEIVED
5 July 2017

REVISED
2 August 2017

ACCEPTED FOR PUBLICATION
10 August 2017

PUBLISHED
14 September 2017

Original content from this work may be used under the terms of the Creative Commons Attribution 3.0 licence.

Any further distribution of this work must maintain attribution to the author(s) and the title of the work, journal citation and DOI.

FAST TRACK COMMUNICATION

Skyrmion production on demand by homogeneous DC currents

Karin Everschor-Sitte[1], **Matthias Sitte**[1], **Thierry Valet**[1], **Artem Abanov**[2] and **Jairo Sinova**[1,3]

[1] Institute of Physics, Johannes Gutenberg University, D-55128 Mainz, Germany
[2] Department of Physics & Astronomy, Texas A&M University, College Station, TX 77843-4242, United States of America
[3] Institute of Physics, Academy of Sciences of the Czech Republic, Cukrovarnicka 10, 162 53 Praha 6, Czechia

E-mail: kaeversc@uni-mainz.de **and** sinova@uni-mainz.de

Keywords: magnetization dynamics, micromagnetic simulations, skyrmions, thin films

Supplementary material for this article is available online

Abstract

Topological magnetic textures—like skyrmions—are major players in the design of next-generation magnetic storage technology due to their stability and the control of their motion by ultra-low currents. A major challenge to develop new skyrmion-based technologies is the controlled creation of magnetic skyrmions without the need of complex setups. We show how to create skyrmions and other magnetic textures in ferromagnetic thin films by means of a homogeneous DC current and without requiring Dzyaloshinskii–Moriya interactions. This is possible by exploiting a static loss of stability arising from the interplay of current-induced spin-transfer-torque and a spatially inhomogeneous magnetization, which can be achieved, e.g., by locally engineering the anisotropy, the magnetic field, or other magnetic interactions. The magnetic textures are created controllably and efficiently with a period that can be tuned by the applied current strength. We propose a specific experimental setup realizable with simple materials, such as cobalt based materials, to observe the periodic formation of skyrmions. We show that adding chiral interactions will not influence the basics of the generations but the consequent dynamics w.r.t. the stabilization of topological textures. Our findings allow for skyrmion production on demand in simple ferromagnetic thin films by homogeneous DC currents.

1. Introduction

Technologies based on spintronics have become integral parts of our world. Current mass-market magnetic memory technologies primarily rely on spintronic devices that couple to the magnetic fields created by domains, which brings inherent limits in storage density and speed. The next-generation, high-performance magnetic memory devices rely on the ability to efficiently and controllably create and manipulate magnetic textures by purely electrical means. Magnetic storage devices based on the racetrack memory idea, where traditionally the information is encoded via magnetic domain walls, has been proposed as a design of ultra-dense, low-cost and low-power storage technologies [1]. However, several difficulties arise to efficiently control the domain walls: (i) large current densities are needed to move them; (ii) nanowires of high quality are required as edge roughness will modify the shape of the domain walls or even destroy them; (iii) the spacing between two magnetic domains can hardly be reduced below about 30 nm [2]; and (iv) longterm thermal stability.

Many challenges related to the structure of the domain walls might be overcome by realizing racetrack memory devices based on magnetic skyrmions [2–5]. They were observed for the first time in 2009 [6] and theoretically discussed already more than 25 years ago [7–9]. Since 2009 skyrmions have been detected in various bulk materials [10–12] and thin films [13–20]. They have also been shown to be stable up to room temperature, and skyrmions occur in different sizes. Skyrmions are particularly interesting for device relevant systems due to their special properties: (i) skyrmions are particle like and are usually repelled by smooth boundaries, so they do not touch the edges of the sample as domain walls always do; (ii) they are topologically non-trivial and therefore more stable than other magnetic textures; (iii) they can be efficiently manipulated by ultra-low electric currents

© 2017 IOP Publishing Ltd and Deutsche Physikalische Gesellschaft

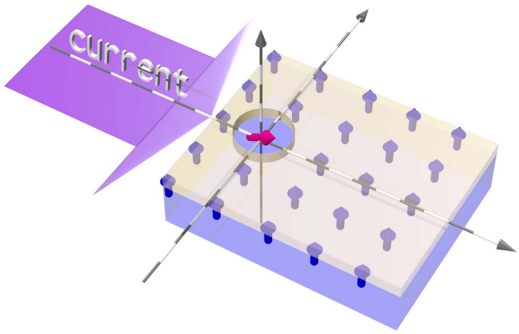

Figure 1. Schematic experimental setup with perpendicular out-of-plane anisotropy in a bilayer thin-film structure, where the anisotropy is modified in a small area via locally modifying the top layer.

[21–26], much smaller than the currents needed to move domain walls in magnetic wires; and (iv) the spacing between bits could be of the order of the skyrmion diameter, which allows for a much denser storage compared to domain walls [2].

To efficiently build high-performance skyrmion-based devices a reliable and controllable way to create skyrmions is needed. So far several techniques to obtain single skyrmions have been proposed [18, 27–39]. However, most of them either require specialized setups or artificially tuned parameters. One recent example is the use of an inhomogeneous current distribution coupled to a chiral Dzyaloshinskii–Moriya interaction (DMI) [30]. This set-up provides a rather uncontrolled skyrmion source where the skyrmion creation is a 'random process' similar to bubble creation in hydrodynamics. Furthermore, most of the theoretical studies of the dynamics [34, 40–52] and creation [35, 39, 53, 54] of these spin textures imply or assume that the presence of a twisting microscopic interactions, such as DMI, is required *for their creation*.

Here we present a mechanism to periodically produce magnetic textures in simple thin film geometries by means of a *homogeneous* DC current and a spatially inhomogeneous magnetization without requiring any standard 'twisting' interactions. To propose a concrete setup we consider an experimentally realizable pinning center, that creates the magnetic inhomogeneity, see figure 1. The magnetic textures can be created efficiently and controllably, as illustrated in figure 2. This mechanism relies physically on a local static loss of stability created by the combined interaction of current-induced spin-transfer torque and the pinning center leading to a bifurcation into a spatio-temporal period pattern. It is similar to our recent work in one dimension leading to current induced domain wall production [55], however in the two-dimensional case the situation is far more complex. We demonstrate that it is possible to use this mechanism to create skyrmion/antiskyrmion pairs. The inclusion of DMI plays no major role in their creation process but does affect the subsequent dynamics of the magnetic textures and in particular ultimately stabilize one member of the pair with the preferred chirality. A recent theoretical study focusing primarily on systems with DMI [56] has also demonstrated the creation of skyrmion/antiskyrmion pairs, also verifying this in the absence of DMI.

This paper is structured as follows: first we provide a simple physical picture of the skyrmion formation. As an example, we explicitly describe an experimental setup in which we predict that skyrmions can be produced via a homogeneous DC current. Then we discuss our main analytical and numerical results. In particular, we consider skyrmion/antiskyrmion pair production and their time evolution and discuss the option of a pulse-operation mode of the device. We first analyze the creation process in a setup without DMI and later on include chiral interactions to study the different time evolution of the created textures. At the end we discuss our results and allude to experiments that might have already observed the creation mechanism proposed in this paper.

2. Physical picture of magnetic texture formation by DC currents

As it follows from the analytics section described below, a DC current is able to produce magnetic textures once there is a magnetic inhomogeneity in the system. To study a concrete and reproducible example, we focus on the setup illustrated in figure 1, consisting of a metallic ferromagnetic film with a perpendicular uniaxial anisotropy where in a small region of the magnetic film the magnetization is tilted. In this work we realize this tilting by a change in the magnetocrystalline anisotropy which acts as a pinning center. We then apply a DC current in an in-plane direction.

The physical picture of the newly introduced mechanism for topological magnetic texture formation is as follows: (i) when ramping up the current strength the current modifies the magnetization structure around the pinning center such that the area, where the magnetization is nonuniform, becomes elongated; (ii) the shape and

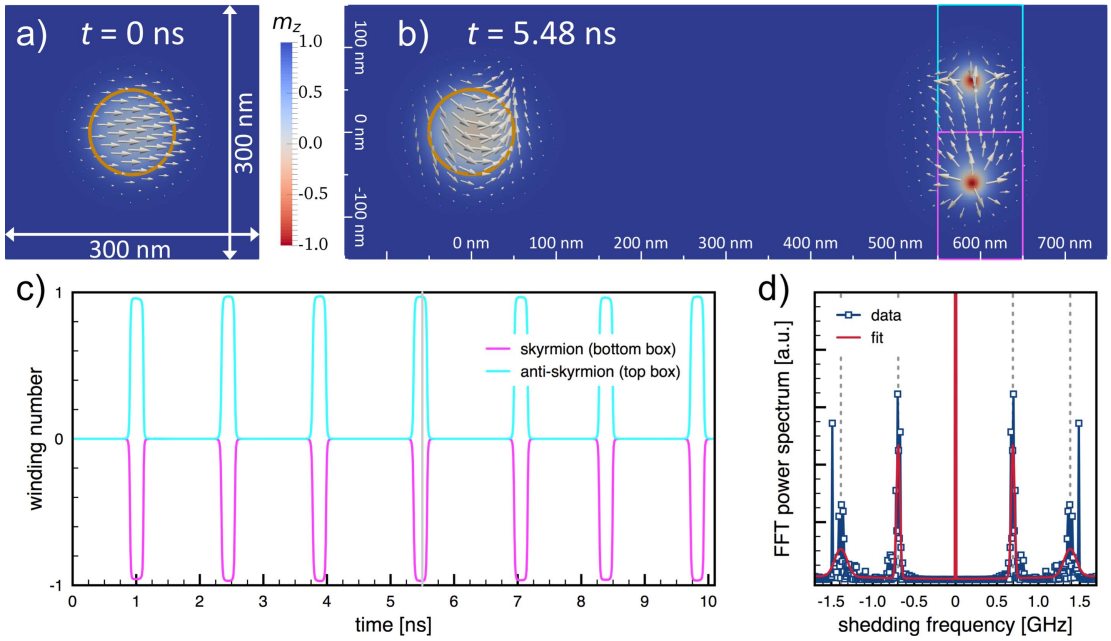

Figure 2. Main results from micromagnetic simulations for the setup of figure 1 where we have chosen material parameters similar to CoCrPt thin films: [57–60] $M_s = 3 \times 10^5$ A m^{-1}, $A_{ex} = 2 \times 10^{-11}$ J m^{-1}, $K_u = 8 \times 10^4$ J m^{-3}, $K_u^p = 0$ and $\tilde{K}_u^p = 1 \times 10^3$ J m^{-3} *inside* the pinning area (indicated by yellow circle) which has a radius of 50 nm, and Gilbert damping of $\alpha = 0.05$, and $\beta = 0$. The applied current density is 5×10^{12} A m^{-2}. (a) Close-up view of the initial magnetization configuration close to the pinning center. The color code indicates the m_z-component, while the arrows visualize the in-plane component of the magnetization. (b) Snapshot of the time evolution under an applied DC current at $t = 5.48$ ns. The skyrmion/antiskyrmion pair exists over a long length of the order of a micrometer. The cyan and magenta boxes indicates regions where we calculate the winding number of each topological object. (c) Winding number of the topological objects as function of time computed over the regions indicated by the box regions in panel (b). (d) Power spectrum of the Fourier transform of the winding number (blue data) and fit (red line) of the peaks up to second harmonic (indicated by dashed gray lines) with a shedding frequency of $f_{shed} \approx 0.68$ GHz.

size of the area of the nonuniform magnetization depends on the strength of the current and microscopic details of the sample. However, since the current couples to the spatial gradient of the magnetization, it acts mainly on the magnetization in the nonuniform area, i.e., near the pinning center; (iii) increasing the current density further, above a critical current density j_c, the local static magnetic texture becomes unstable and the current-induced spin-transfer-torque pushes away the nucleated texture and effectively shed it from the pinning center; (iv) the vicinity of the pinning center is then somewhat restored to its initial state, and the process can restart, leading to a periodic shedding process if the current is kept constant above j_c. Here we would like to stress that the current density above which the ferromagnetic ground state becomes unstable is higher than the current densities used to obtain the shedding [55, 61, 62].

The above statements (i) can be deduced from the analytics part presented in section 4, (ii) are analogous to the one dimensional case [55, 62], and (iii) can be deduced from a more general perspective from hydrodynamic theory [63]. However what remains unclear from those general arguments is how these shedded magnetic textures look like. To this end we have performed micromagneticsimulations and we find that different magnetic textures can be shedded (see Supplementary material is available online at stacks.iop.org/NJP/19/092001/mmedia.). In particular, for currents slightly above j_c and a small enough pinning center it is possible to periodically shed skyrmion/antiskyrmion pairs.

In the process described above, no twisting interaction is needed. The addition of DMI would not aid or hinder the periodic creation process of magnetic textures, but will of course be necessary in a different region of the device to insure long term stability of stored skyrmions, see section 5.2. It is important to emphasize that the newly introduced periodic texture production mechanism is a generic and ubiquitous process: neither the directions of the anisotropies nor the details of how it is locally altered in strength or orientation at the pinning center are crucial. However, in order to demonstrate the practical feasibility of the proposed generic mechanism, we have specified an experimental setup based on CoCrPt thin films [57–60] to observe the formation of skyrmions by uniform DC currents in common ferromagnetic materials, as shown in figure 1. Locally modifying the top layer in a small region might reduce the out-of-plane anisotropy leading to an in-plane tilting of the magnetization within this region, as a practical implementation of the required local pinning center.

3. Model for magnetization dynamics

To describe the current-induced magnetization dynamics of the considered ferromagnetic thin film we use the Landau–Lifshitz–Gilbert equation for the unit vector field $\hat{\boldsymbol{M}}$ [64] generalized to include spin-torque effects due to the electric current:

$$(\partial_t + v_s\partial_x)\hat{\boldsymbol{M}} = -\gamma\hat{\boldsymbol{M}} \times \boldsymbol{B}_{\text{eff}} + \alpha\hat{\boldsymbol{M}} \times \left(\partial_t + \frac{\beta}{\alpha}v_s\partial_x\right)\hat{\boldsymbol{M}}, \tag{1}$$

where γ is the gyromagnetic ratio, and α and β are the dimensionless Gilbert damping and non-adiabatic spin-transfer-torque parameters. The effective magnetic field is given by $\boldsymbol{B}_{\text{eff}} = -M_s^{-1}(\delta F[\hat{\boldsymbol{M}}]/\delta\hat{\boldsymbol{M}})$, where $F[\hat{\boldsymbol{M}}]$ describes the free energy of the system and M_s is the saturation magnetization. We decompose the free energy F into two parts $F = F_0 + F_{\text{twist}}$ where F_0 consists of isotropic exchange, anisotropy term and dipolar interactions:

$$F_0[\hat{\boldsymbol{M}}] = \int\left[A_{\text{ex}}(\nabla\hat{\boldsymbol{M}})^2 + \Pi(\hat{\boldsymbol{M}}) - \frac{\mu_0}{2}M_s\hat{\boldsymbol{M}} \cdot \boldsymbol{H}_d(\hat{\boldsymbol{M}})\right]\mathrm{d}V, \tag{2}$$

where A_{ex} is the exchange constant, $\Pi(\hat{\boldsymbol{M}})$ describes the functional form of the anisotropy energy and the last term describes the dipolar interactions. F_{twist} describes a twisting interaction like DMI, which we set to zero in the first part of the numerics. Thereby we show that such a twisting term is not crucial for the creation of the magnetic textures. In the latter part of the numerics we do, however, explicitly consider different twisting terms The applied uniform DC current along the x direction enters the equation via the effective spin velocity, $v_s = \xi j$ with $\xi = gP\mu_B/(2eM_s)$, where g is the g-factor, P is the current polarization, μ_B is the Bohr magneton, e is the electron charge, and j is the current.

4. Results: analytics

In this section we demonstrate the general aspects of this new type of magnetic texture production in thin films. We show below that spin textures are periodically created above a critical current j_c, with a period $T \sim (j - j_c)^{-1/2}$. This periodic texture production is quite general and does not depend on the details of the microscopic Hamiltonian for a large class of magnetic systems. However, the details of the process, such as the value of the critical current j_c or the prefactor of the periodic scaling, do depend on the microscopic details of the Hamiltonian. Recently we have analyzed the same mechanism for one-dimensional nano-wires [55], where a pinning center leads to current-induced periodic domain wall production. The one-dimensional problem is analytically solvable including the calculation of the shape of the emerging magnetic texture of the domain wall, whereas the situation in two dimensions is far more complex. Analytically it is still possible to derive the shedding period based on generalized arguments as shown below. By general topology arguments one can infer that the winding number during the creation process is conserved, but the precise shape of the produced magnetic textures cannot be calculated analytically.

The only assumptions that enter our analytical calculations are that (i) the magnetic free energy density of the system is translationally invariant outside the pinning area, and (ii) that we neglect the non-adiabatic spin-transfer torque term. The critical scaling related to the type of instability may be transformed by non-adiabatic corrections, but the general finding of periodic production of spin textures by DC currents is expected to remain valid. Below we discuss the main analytical strategy and findings, whereas a full derivation of our analytical results can be found in the supplementary material (see footnote 4).

The critical current density is defined by the instance when the magnetic texture is about to rip off. Because the current density couples to the gradient of the magnetization via the spin-transfer torque, the critical current density is defined by the gradient of the magnetization profile at the pinning center going to zero:

$$\partial_x\hat{\boldsymbol{M}}_c(j_c; \boldsymbol{r} = 0) = 0, \tag{3}$$

where $\hat{\boldsymbol{M}}_c(\boldsymbol{r})$ is the magnetization profile obtained by solving the Landau–Lifshitz–Gilbert equation for a current density j_c. A sketch of the magnetization profile for different current strengths is shown in figure 3.

The period at which magnetic textures are created is derived by combining two crucial arguments: one arises from the 'just still static limit' ($j_0 \lesssim j_c$) and the other one from the 'just dynamic limit' ($j \gtrsim j_c$). For the first one, the crucial point to note is that at a current j_0 slightly smaller than the critical current ($j_0 \lesssim j_c$) the magnetization profile will not differ too much from the critical one besides being shifted by a small distance x_0: $\hat{\boldsymbol{M}}_0(\boldsymbol{r}) \equiv \hat{\boldsymbol{M}}_c(\boldsymbol{r} - x_0\boldsymbol{e}_x) + \delta\hat{\boldsymbol{M}}$. Solving the LLG in the static limit with this ansatz yields

$$j_c - j_0 \sim x_0^2. \tag{4}$$

This equation establishes the relation between the spatial shift of the critical solution, x_0, and the current j_0. As a check we note that (i) for $x_0 = 0$, j_0 and the critical current j_c coincide, and that (ii) the difference $j_c - j_0$ is second order in x_0, as expected from perturbation theory arguments.

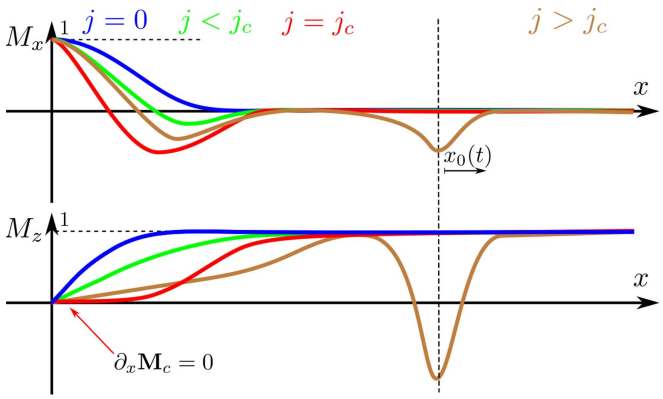

Figure 3. Schematic plot for which the local pinning direction is along the x direction, and the global pinning direction is along the z direction, i.e., $M_x(x = 0) = 1$ for all current strengths. At the critical current all derivatives at $x = 0$ are zero.

For currents just larger than the critical current j_c, the static solutions are unstable. Therefore, to obtain information about the dynamics of the magnetization configuration, a justified ansatz for the magnetization at an applied current j is a sum of $\boldsymbol{M}_0$ (with a time dependent shift x_0) and a small perturbation: $\boldsymbol{M}(\boldsymbol{r}, t) = \boldsymbol{M}_0(\boldsymbol{r}; x_0(t)) + \boldsymbol{m}(\boldsymbol{r}, t)$. Here, $\boldsymbol{M}_0(\boldsymbol{r})$ is the static magnetization configuration for the shift x_0 which can be parameterized by a current j_0 using equation (4). For this ansatz, the Landau–Lifshitz–Gilbert equation has a direct solution with $\boldsymbol{m} \equiv 0$ and

$$\partial_t x_0 = j - j_0, \tag{5}$$

implying that the velocity of the magnetic texture is proportional to the applied current.

Solving equation (4) for j_0 and inserting it in equation (5) yields the period of the magnetic texture formation:

$$T \sim (j - j_c)^{-1/2}. \tag{6}$$

5. Results: numerics

We have performed micromagnetic simulations with various setups and various configurations, using both MicroMagnum [65] including additional self-written software extensions as well as MuMax3 [66]. For details and parameters used see the Methods section (section 8) and for a summary table of the parameters see the supplementary material (see footnote 4). In the first part we focus on the periodic texture formation, in particular on the skyrmion and anti-skyrmion creation itself and try to isolate the mechanism to show that DMI is not important for their creation. We analyze the shedding and the time evolution. After that we consider the shedding process in the presence of the generalized anisotropic DMI [67, 68] which after the skyrmion and antiskyrmion pairs are created, support the stabilization of the skyrmion or the antiskyrmion, depending on the details and the signs of the entries of the DMI tensor, respectively.

In the following we will present our simulation results for a DC current which is ramped up to a constant value above j_c, where we have used the following form of the anisotropy term:

$$\Pi(\hat{\boldsymbol{M}}) = \begin{cases} K_u(1 - M_z^2), & \text{for the film,} \\ K_u^{\mathrm{p}}(1 - M_z^2) + \tilde{K}_u^{\mathrm{p}}(1 - M_x^2), & \text{in the pinning center.} \end{cases} \tag{7}$$

We assume that in the pinning center the anisotropy strength K_u^{p} is reduced, i.e., $K_u^{\mathrm{p}} < K_u$, such that the corresponding effective anisotropy in the ultrathin film limit induced by the dipolar interactions ($K_{\mathrm{eff}} = K - (\mu_0/2)M_s^2$) is positive (negative) for K_u (K_u^{p}). This effectively leads to a tilting of the magnetic texture into the plane within the pinning region. Since in a real material there is always a small uniaxial anisotropy also in an in-plane direction, we have taken a small rotational symmetry breaking term into account, tilting the magnetic texture along x direction. This corresponds for example to the setup depicted schematically in figure 1.

In the supplementary material we present additional results: (i) for simulations even without dipolar interactions, in which a skyrmion and an antiskyrmion are energetically fully equivalent wherefore the creation and decay process for skyrmions and antiskyrmions is fully symmetric; (ii) for the creation of different magnetic textures; and (iii) a pulse operation mode of the 'device'.

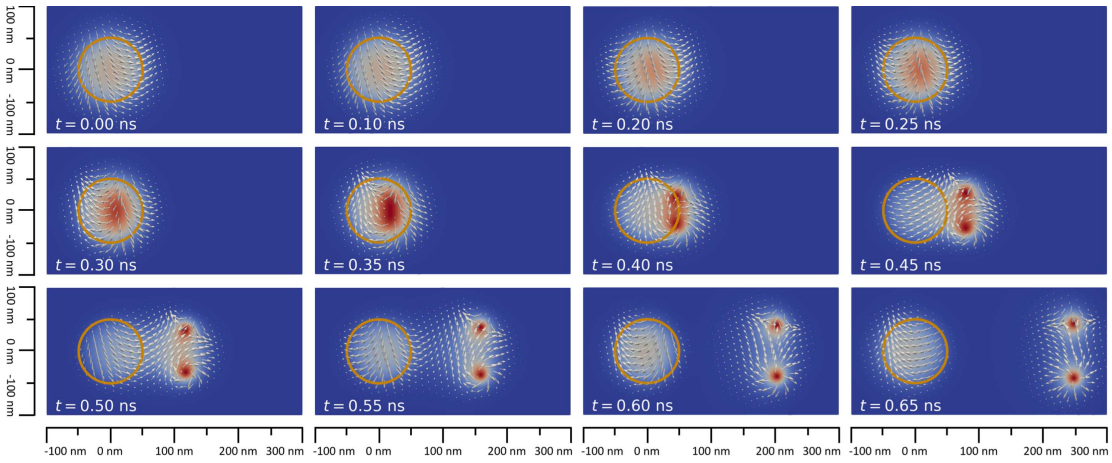

Figure 4. Details of the shedding process of the time evolution of a skyrmion/antiskyrmion pair shown in figure 2. Shown is the z component as a color code, and the arrows visualize the in-plane components. For this setup, we use the same parameters as in figure 2: $M_s = 3 \times 10^5$ A m^{-1}, $A_{ex} = 2 \times 10^{-11}$ J m^{-1}, $K_u = 8 \times 10^4$ J m^{-3}, $K_u^p = 0$ and $\tilde{K}_u^p = 1 \times 10^3$ J m^{-3} *inside* the pinning area which has a radius of 50 nm, Gilbert damping of $\alpha = 0.05$, and $\beta = 0$. The applied current density is 5×10^{12} A m^{-2}.

5.1. Numerics without DMI

A typical relaxed magnetization configuration is shown in figure 2(a). In the continuous operation mode, a DC current above the critical one can generate periodically spin textures. For a large set of parameters these spin textures evolve into skyrmion/antiskyrmion pairs. A typical snapshot for the time evolution of the magnetization under a (continuous) DC current is presented in figure 2(b). To establish the topological nature of the skyrmion and antiskyrmion we have calculated as a function of time the winding numbers over spatial regions indicated by the boxes in cyan and magenta. The results presented in panel (c) clearly show a period creation of skyrmion/antiskyrmion pairs with winding numbers ± 1. The shedding frequency for the simulated material structure with applied current density of 5×10^{12} A m^{-2} can be extracted from the power spectrum of the Fourier transformed data, $\omega_{shed} \approx 0.68$ GHz corresponding to a shedding period of approximately $T_{shed} \approx 1.47$ ns (see panel (d)). For this setup, we have used $M_s = 3 \times 10^5$ A m^{-1}, $A_{ex} = 2 \times 10^{-11}$ J m^{-1}, $K_u = 8 \times 10^4$ J m^{-3}, $K_u^p = 0$ and $\tilde{K}_u^p = 1 \times 10^3$ J m^{-3} *inside* the pinning area which has a radius of 50 nm, and Gilbert damping of $\alpha = 0.05$, and $\beta = 0$. More information on the numerical part can be found in the Methods section, section 8.

5.1.1. Shedding of skyrmion/antiskyrmion pairs

For currents less than the critical current, the magnetic texture around the pinning center elongates until above the critical current it breaks off and a first skyrmion/antiskyrmion pair is formed, which travels along the magnetic film. The details of the shedding process are shown in figure 4, where we show the profiles of the pinning center up to 0.65 ns. The observation that the created topological texture comes in a pair with opposite topological charge reflects the fact that during the creation process the topological charge is conserved, with initial configuration having no topological charge.

5.1.2. Time-evolution of a skyrmion/antiskyrmion pair

The skyrmion/antiskyrmion pair begins to move away from the pinning center and we observe in our simulations that the distance between the anti-skyrmion and skyrmion increases at a rate proportional to α as expected (with $\beta = 0$ in our simulations). The evolution of the pair has an oscillatory character related to the fact that, in equilibrium, the individual structures are not stable. This is shown in detail in figure 5. The dynamical stabilization due to the current leads to the global continuous precession of all spins around the z axis. This results in the skyrmion (lower magnetic texture) oscillating continuously between Néel and Bloch skyrmion type and between negative and positive chirality, as discussed in [31], and to the anti-skyrmion (upper magnetic texture) rotating its orientation counterclockwise. For the modeled setup we obtain an oscillation frequency of $f_{osc} \approx 1/0.34$ ns ≈ 2.9 GHz being about four times faster than the shedding frequency. This oscillatory behavior does depend on the details of the specific sample and therefore we do not explore it further, since it does not affect the production or control of the texture in the considered time and length scale.

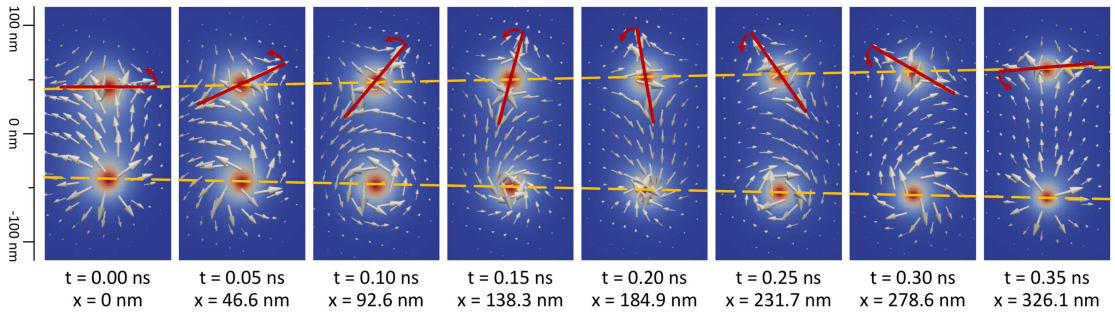

Figure 5. Detailed time evolution of a skyrmion/antiskyrmion pair in time steps of 0.05 ns. The skyrmion (lower configuration) oscillates continuously in time from a Bloch to a Néel skyrmion and from positive to negative chirality [31]. Here all spins globally rotate counterclockwise in time. The same applies for the antiskyrmion (upper configuration), leading to a continuous counterclockwise rotation of the red line (serving as guide to the eye) at which the spins are pointing away from the center of the antiskyrmion. The oscillation frequency is $f_{\mathrm{osc}} \approx 1/0.34$ ns ≈ 2.9 GHz. The dashed yellow lines visualize the drift in opposite directions in y direction due to opposite Magnus forces for skyrmion and antiskyrmion. For this setup, we used the same parameters as in figure 2: $M_{\mathrm{s}} = 3 \times 10^5$ A m^{-1}, $A_{\mathrm{ex}} = 2 \times 10^{-11}$ J m^{-1}, $K_u = 8 \times 10^4$ J m^{-3}, $K_u^{\mathrm{p}} = 0$ and $\tilde{K}_u^{\mathrm{p}} = 1 \times 10^3$ J m^{-3} *inside* the pinning area which has a radius of 50 nm, and Gilbert damping of $\alpha = 0.05$, and $\beta = 0$. Applied current is 5×10^{12} A m^{-2}.

5.1.3. Decay of magnetic textures

In presence of a non-zero Gilbert damping, the created topological textures which are dynamical solitons [31, 69], progressively decay (their radius shrinks) at a rate proportional to α. They will ultimately collapse in a finite time due to imperfect topological protection on a lattice, unless they reach an area with non zero chiral interaction at which place either the skyrmion or the antiskyrmion is meta-stable allowing for longer term storage.

In the presented examples the skyrmion and anti-skyrmion do not decay at the same time. In the presence of dipolar interactions, which do not break the rotational symmetry, a skyrmion is energetically favored compared to the antiskyrmion, resulting in principle in a slightly larger life time. However, the shedding process itself, the oscillation of the magnetic textures, as well as their decay create a non-negligible amount of spin waves, which in turn influence the time evolution of the magnetic textures in the system. Therefore, a complete understanding of a certain decay process does depend on the history of the system. In our micromagnetic simulations we indeed observe instances where either the skyrmion or the antiskyrmion decays first as can be seen in figure 6, where the top and bottom row are taken from the same simulation just at different times. In the supplementary material (see footnote 4) we consider also a system without dipolar interactions where neither skyrmion nor antiskyrmion are favored and we observe that they decay at the same time.

5.2. Numerics with anisotropic DMI

The simulations presented above were intentionally performed without chiral interactions to explore the creation mechanism. For the stabilization of chiral magnetic textures, however, an inversion asymmetric interaction is needed. In the following, we consider the creation mechanism in the presence of anisotropic Néel DMI: [67, 68]

$$F_{\mathrm{twist}} = \int \left[D_1 \left(M_x \frac{\partial M_z}{\partial x} - M_z \frac{\partial M_x}{\partial x} \right) + D_2 \left(M_y \frac{\partial M_z}{\partial y} - M_z \frac{\partial M_y}{\partial y} \right) \right] \mathrm{d}V. \tag{8}$$

For $D_1 = D_2 = D$, the twisting energy F_{twist} describes the standard Néel DMI [70] favouring magnetic skyrmions. For $\mathrm{sign}(D_1/D_2) = +1$ a skyrmion like configuration is still energetically more favorable, whereas for $\mathrm{sign}(D_1/D_2) = -1$ an antiskyrmion like configuration will have a lower energy compared to a skyrmion like texture [67, 68]. Anti-skyrmions have been studied, but until recently they have often been considered as unstable objects [51]. More recent works show that anti-skyrmions can also occur as (meta-)stable states [67, 68, 71].

Simulation results with anisotropic DMI are shown in figure 7. Here, skyrmion and anti-skyrmion pairs are created as previously, however, the time evolution for the pairs is now influenced by the DMI. In the upper (lower) row in figure 7 we considered a DMI with $D_1 = 5 \times 10^4$ J m^{-2} and $D_2 = \pm D_1$, which optimally favor a symmetric skyrmion (antiskyrmion).

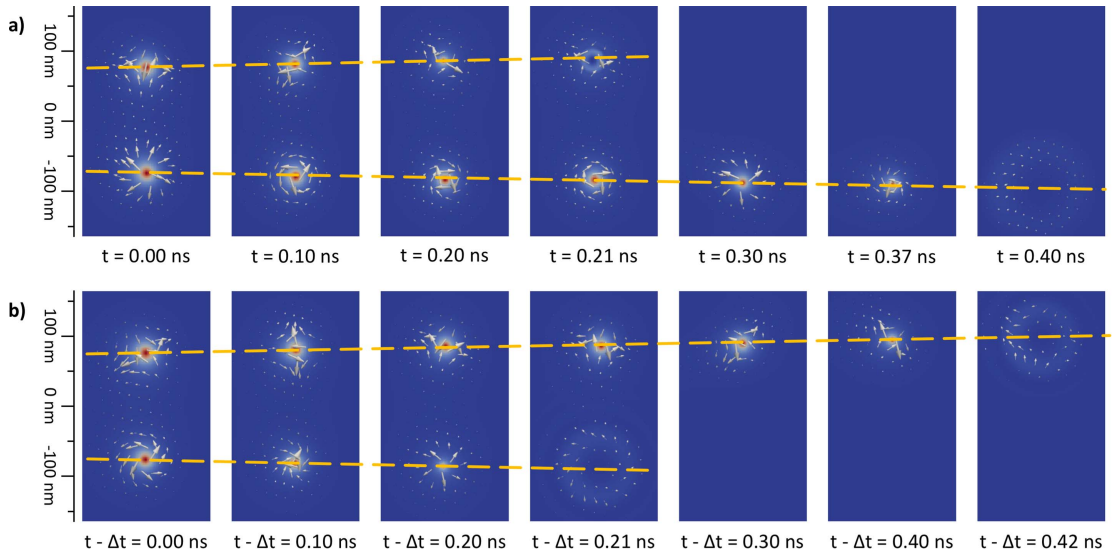

Figure 6. Snapshot of the time evolution of a skyrmion/antiskyrmion pair where in the upper panel (a) (lower panel (b)) the antiskyrmion (skyrmion) decays faster than the skyrmion (antiskyrmion) due to interactions with spin waves generated by previous skyrmion/antiskyrmion pairs. Note that the top and bottom panel are taken from the same simulation, but from different pairs created at different times. The event shown in panel (b) occurs about $\Delta t = 3$ ns later. Furthermore, the two events are not fully symmetric and do depend on the history of the system. For this setup, we used the same parameters as in figure 2: $M_s = 3 \times 10^5$ A m^{-1}, $A_{ex} = 2 \times 10^{-11}$ J m^{-1}, $K_u = 8 \times 10^4$ J m^{-3}, $K_u^p = 0$ and $\tilde{K}_u^p = 1 \times 10^3$ J m^{-3} *inside* the pinning area which has a radius of 50 nm, and Gilbert damping of $\alpha = 0.05$, and $\beta = 0$. Applied current is 5×10^{12} A m^{-2}.

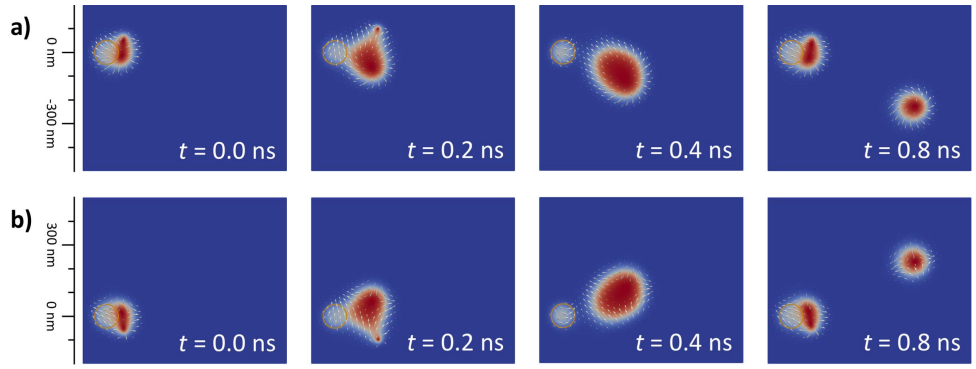

Figure 7. Upper row: time evolution for $D_1 = D_2 = 5 \times 10^4$ J m^{-2} corresponding to the DC current density $j = 3.25 \times 10^{12}$ A m^{-2}. Again there is a production of skyrmion/antiskyrmion pairs, however during time evolution the skyrmion texture is preferred. Lower row: time evolution for $D_1 = -D_2 = 5 \times 10^4$ J m^{-2}. Here, in contrast to normal DMI, the anti-skyrmion texture is preferred by the anti-DMI.

6. Discussion

The process that we have described is an alternative way to controllably produce skyrmions and also antiskyrmions periodically. Whereas the process itself is quite general given a set of simple restrictions (a pinned magnetic inhomogeneity in the system caused by, for example, a local change in the anisotropy), the specific values of the critical current are set by the material properties. For the examples chosen the current densities are typical of the spin-transfer torque process. Although this implies the need for large current densities, leading to possible Joule heating, this heating can be mitigated experimentally by applying pulses, see supplementary material (see footnote 4). Such heating does not alter the general conclusions and just renormalizes some of the material-dependent parameters.

The incorporation of a twisting interaction like (anisotropic) DMI is not essential for the physics of the skyrmion/antiskyrmion pair *creation* process described here. It affects the value of the critical current and the shape of textures generated. In addition it helps towards a stabilization for the created (anti-)skyrmion texture in the static case. Hence, there is no contradiction with the Derrick–Hobart theorem [72, 73] that states that there is no nontrivial localized static solution for skyrmion without chiral interactions. In our process, which we believe

is similar to the one obtained in [56], dynamic skyrmions and antiskyrmions are being produced, and could be stabilized at a later stage in regions with non zero (anisotropic) DMI.

In prior studies, several techniques to obtain single skyrmions have been proposed [18, 27–33]. However, most of them either require specialized setups or artificially tuned parameters. One recent example is the use of an inhomogeneous current distribution in the presence of DMI [30]. It is also possible to create magnetic skyrmions by an electric current in a sample with a suitable kink subject to DM interactions due to the divergence of the magnetization in the corner [41]. In particular, here the authors observe an asymmetry in the current, meaning that they do not create skyrmions when the current is flowing in the opposite direction. Recent numerical simulation studies show that a skyrmion can be created by the local injection of a spin-polarized current perpendicular to the plane [31, 74]. In [31] the authors also produce skyrmions in a setup without DMI, however they require a specialized setup with a nanocontact and the process is not connected to the periodic shedding created by the interaction between the current and the locally modified anisotropy as we propose here.

While these processes will be explored in the near future by experimental groups in search for efficient ways of controllably creating skyrmions, we propose a more general method that is applicable to systems readily available to a wider group of experimentalist.

We believe that the creation process discussed here has already been observed in recent experiment in variant setups, e.g., an injection of skyrmions is by DC current pulses [35–37, 39]. In [35] the authors report a nucleation of skyrmions with a current pulse at the tip of a needle-like current injecting electrode. Here, the Oersted field near the tip may act as a dynamically defined pinning center similar to what we consider here. In [36], we speculate that the grains in the sample are responsible for creating local inhomogeneities in the magnetization, i.e., induce pinning centers. When a DC current is applied, at those points skyrmion and anti-skyrmion pairs will be created.

In [39] the authors use sub-nanosecond spin-orbit torque pulses to generate single skyrmions based on the concept of having a reduced anisotropy in a certain region of the sample, as we propose in our work.

Since in all of these works [35–37] DMI is present in the considered systems, the antiskyrmions will die quickly on timescales that are not in the experimental accessible range in the measurement setup that have been reported so far.

To experimentally verify our prediction we suggest the following: (i) one of the key aspects of our mechanism is that it generates a periodic shedding of magnetic textures with a period that can be tuned by current strength, when applying a DC current. In the above mentioned experiments, current pulses have been applied. When increasing the length of the current pulses towards having effectively a DC current, it might be possible to measure the current dependent period. (ii) The other key aspect in our theory is the magnetic inhomogeneity. By increase locally the inhomogeneities at a certain point of the sample we predict that skyrmions can be produced in this region already with lower current densities. Examples to do so would be to have a small area where the sample is thinner or thicker. Alternatively, one can put a magnetic impurity into the system but the effect of the magnetic impurity may be harder to control.

7. Conclusions

In this work we have demonstrated that it is possible to create magnetic textures by uniform DC electric currents without the need of a magnetic field or any standard 'twisting' interactions like Dzyaloshinskii–Moriya. We have shown that skyrmion and antiskyrmion pairs can be created efficiently, controllably and periodically where the period can be tuned by the applied current strength. We analytically derived, that in the limit of vanishing non-adiabatic torque, the period T of production near the critical current has a dependence $T \sim (j - j_c)^{-1/2}$, arising from quite general grounds based on simple symmetry consideration of the governing dynamic equations. In principle, within a pulse operation mode skyrmions can be produced on demand. This provides a new avenue to study the *creation* of topological magnetic textures by electric means in simple geometries. Adding DMI helps to stabilize magnetic skyrmions.

8. Micromagnetic simulations

Micromagnetic simulations were performed based on MicroMagnum [65] including additional self-written software extensions and MuMax3 [66]. In the simulations shown in this article we have simulated a quasi-two-dimensional thin film with lateral dimensions $2\ \mu\text{m} \times 1\ \mu\text{m} \times 1$ nm consisting of $1000 \times 500 \times 1$ cells in x, y, and z direction, respectively, which corresponds to discretization length of 2 nm in x and y directions and 1 nm in z direction. For the plots shown in this manuscript we have chosen material parameters similar to CoCrPt thin films with perpendicular magnetic anisotropy: [57–60] $M_s = 3 \times 10^5 \text{A m}^{-1}$, $A_{ex} = 2 \times 10^{-11} \text{J m}^{-1}$, and out-of-plane anisotropy $K_u = 2 \times 10^4 \text{ J m}^{-3}$ with anisotropy energy functional $\Pi(\boldsymbol{M}) = 1 - M_z^2$. The pinning center is

modeled as a cylinder along z direction with a radius of 50 nm and reduced anisotropy $K_u = 0$ in z direction, but $\tilde{K}_u^{\mathrm{p}} = 1 \times 10^3$ J m^{-3} in x direction breaking the in-plane rotational symmetry.

Before applying any DC currents we have first relaxed the system to the ground state using a large Gilbert damping parameter of $\alpha = 0.25$. Subsequent simulations were performed with $\alpha = 0.05$, except when noted otherwise. In all simulations we have set the non-adiabatic spin-torque parameter to zero, $\beta = 0$. We have checked that the results are independent of the grid sizes.

Our simulations were performed at zero temperature. We expect that the mechanism of shedding magnetic textures will be robust against thermal fluctuations [31] and the qualitative picture will of the creation mechanism will not change as (i) the energy scale corresponding to the thermal fluctuations are expected to be smaller than the ones from the current [75], and (ii) thermal effects are isotropic. However, we do expect that the subsequent dynamics of the shedded magnetic textures will be affected by thermal fluctuations. In particular the accompanied emission of magnons will cause the shedded magnetic textures to interact with themselves and the boundaries of the sample.

Acknowledgments

We are grateful to M Thorwart, M Stier, O Gomonay, K Litzius, A Rosch, and K Hals for discussions. Ar A is also very grateful for the warm hospitality of the supporting staff of the INSPIRE group at Johannes Gutenberg-Universität, Mainz, Germany. We acknowledge the funding from the Alexander von Humboldt Foundation, the Transregional Collaborative Research Center (SFB/TRR) 173 Spin+X, and the ERC Synergy Grant SC2 (No. 610115). KE-S acknowledges funding from the German Research Foundation (DFG) under the Project No. EV 196/2-1.

Author contributions

Ar A, KE-S, TV, and JS did the planning of the project. Ar A initiated the project and performed the analytic calculations. TV proposed device configurations. MS, and KE-S performed the numerical calculations. All the authors contributed to the writing of the manuscript.

ORCID iDs

Karin Everschor-Sitte https://orcid.org/0000-0001-8767-6633
Matthias Sitte https://orcid.org/0000-0001-6004-7861
Jairo Sinova https://orcid.org/0000-0002-9490-2333

References

[1] Parkin S S P, Hayashi M and Thomas L 2008 *Science* **320** 190–4
[2] Fert A, Cros V and Sampaio J 2013 *Nat. Nanotechnol.* **8** 152–6
[3] Tomasello R, Martinez E, Zivieri R, Torres L, Carpentieri M and Finocchio G 2014 *Sci. Rep.* **4** 6784
[4] Zhang X, Zhao G P, Fangohr H, Liu J P, Xia W X, Xia J and Morvan F J 2015 *Sci. Rep.* **5** 7643
[5] Müller J 2017 *New J. Phys.* **19** 025002
[6] Mühlbauer S, Binz B, Jonietz F, Pfleiderer C, Rosch A, Neubauer A, Georgii R and Böni P 2009 *Science* **323** 915–20
[7] Pokrovsky V 1979 *Adv. Phys.* **28** 595–656
[8] Bogdanov A N and Yablonskii D 1989 *Zh. Eksp. Teor. Fiz.* **95** 178
[9] Bogdanov A N and Hubert A 1994 *J. Magn. Magn. Mater.* **138** 255–69
[10] Pfleiderer C *et al* 2010 *J. Phys. Condens. Matter* **22** 164207
[11] Seki S, Yu X Z, Ishiwata S and Tokura Y 2012 *Science* **336** 198–201
[12] Adams T, Chacon A, Wagner M, Bauer A, Brandl G, Pedersen B, Berger H, Lemmens P and Pfleiderer C 2012 *Phys. Rev. Lett.* **108** 1–5
[13] Yu X Z, Onose Y, Kanazawa N, Park J H, Han J H, Matsui Y, Nagaosa N and Tokura Y 2010 *Nature* **465** 901–4
[14] Yu X Z, Kanazawa N, Onose Y, Kimoto K, Zhang W Z, Ishiwata S, Matsui Y and Tokura Y 2011 *Nat. Mater.* **10** 106–9
[15] Yu X, Kanazawa N, Zhang W, Nagai T, Hara T, Kimoto K, Matsui Y, Onose Y and Tokura Y 2012 *Nat. Commun.* **3** 988
[16] Heinze S, von Bergmann K, Menzel M, Brede J, Kubetzka A, Wiesendanger R, Bihlmayer G and Blügel S 2011 *Nat. Phys.* **7** 713–8
[17] Onose Y, Okamura Y, Seki S, Ishiwata S and Tokura Y 2012 *Phys. Rev. Lett.* **109** 037603
[18] Romming N, Hanneken C, Menzel M, Bickel J E, Wolter B, von Bergmann K, Kubetzka A and Wiesendanger R 2013 *Science* **341** 636–9
[19] Moreau-Luchaire C *et al* 2016 *Nat. Nanotechnol.* **11** 444–8
[20] Woo S *et al* 2016 *Nat. Mater.* **15** 501–6
[21] Jonietz F *et al* 2010 *Science* **330** 1648–51
[22] Schulz T, Ritz R, Bauer A, Halder M, Wagner M, Franz C, Pfleiderer C, Everschor K, Garst M and Rosch A 2012 *Nat. Phys.* **8** 301–4
[23] Everschor K 2012 Current-induced dynamics of chiral magnetic structures *PhD Thesis* University of Cologne
[24] Nagaosa N and Tokura Y 2013 *Nat. Nanotechnol.* **8** 899–911
[25] Litzius K *et al* 2017 *Nat. Phys.* **13** 170–5

[26] Jiang W et al 2017 Nat. Phys. 13 162
[27] Mohseni S M et al 2013 Science 339 1295
[28] Zhou Y and Ezawa M 2014 Nat. Commun. 5 4652
[29] Li J et al 2014 Nat. Commun. 5 4704
[30] Jiang W et al 2015 Science 349 283–6
[31] Zhou Y, Iacocca E, Awad A A, Dumas R K, Zhang F C, Braun H B and Akerman J 2015 Nat. Commun. 6 8193
[32] Yuan H Y and Wang X R 2016 Sci. Rep. 6 22638
[33] Müller J, Rosch A and Garst M 2016 New J. Phys. 18 065006
[34] Heinonen O, Jiang W, Somaily H, te Velthuis S G E and Hoffmann A 2016 Phys. Rev. B 93 094407
[35] Hrabec A, Sampaio J, Belmeguenai M, Gross I, Weil R, Chérif S M, Stashkevich A, Jacques V, Thiaville A and Rohart S 2017 Nat. Commun. 8 15765
[36] Legrand W, Maccariello D, Reyren N, Garcia K, Moutafis C, Moreau-Luchaire C, Collin S, Bouzehouane K, Cros V and Fert A 2017 Nano Lett. 17 2703–12
[37] Hoffmann A 2017 Presentation at DPG Meeting
[38] Yu X et al 2017 Adv. Mater. 29 1606178
[39] Büttner F et al 2017 arXiv:1705.01927
[40] Han J H, Zang J, Yang Z, Park J H and Nagaosa N 2010 Phys. Rev. B 82 94429
[41] Iwasaki J, Mochizuki M and Nagaosa N 2013 Nat. Commun. 4 1463
[42] Petrova O and Tchernyshyov O 2011 Phys. Rev. B 84 214433
[43] Kalinkin A and Skorikov V 2011 Inorg. Mater. 47 63–7
[44] Liu R, Lim W and Urazhdin S 2013 Phys. Rev. Lett. 110 147601
[45] Iwasaki J, Beekman A J and Nagaosa N 2014 Phys. Rev. B 89 064412
[46] Tchoe Y and Han J H 2012 Phys. Rev. B 85 174416
[47] Tretiakov O A and Tchernyshyov O 2007 Phys. Rev. B 75 012408
[48] Iwasaki J, Mochizuki M and Nagaosa N 2013 Nat. Nanotechnol. 8 742–7
[49] Roessler U K, Bogdanov A N, Pfleiderer C and Rößler U K 2006 Nature 442 797–801
[50] Mochizuki M 2012 Phys. Rev. Lett. 108 017601
[51] Koshibae W and Nagaosa N 2016 Nat. Commun. 7 10542
[52] Leonov A O and Mostovoy M 2017 Nat. Commun. 8 14394
[53] Lin C C, Penumatcha A V, Gao Y, Diep V Q, Appenzeller J and Chen Z 2013 Nano Lett. 13 5177–81
[54] Lin S Z, Batista C D and Saxena A 2014 Phys. Rev. B 89 024415
[55] Sitte M, Everschor-Sitte K, Valet T, Rodrigues D R, Sinova J and Abanov A 2016 Phys. Rev. B 94 064422
[56] Stier M, Häusler W, Posske T, Gurski G and Thorwart M 2017 Phys. Rev. Lett. 118 267203
[57] Zheng Y F, Wang J P and Ng V 2002 J. Appl. Phys. 91 8007
[58] Roy A G, Nuhfer N T and Laughlin D E 2003 J. Appl. Phys. 93 8179–81
[59] Navas D, Nam C, Velazquez D and Ross C A 2010 Phys. Rev. B 81 1–11
[60] Kane M M 2015 Fabrication and characterization of perpendicular magnetic anisotropy thin-film CoCrPt grown on a Ti underlayer BSc Thesis Massachusetts Institute of Technology (https://dspace.mit.edu/handle/1721.1/98555)
[61] Bazaliy Y B, Jones B A and Zhang S C 1998 Phys. Rev. B 57 R3213
[62] Shibata J, Tatara G and Kohno H 2005 Phys. Rev. Lett. 94 076601
[63] Iacocca E and Hoefer M A 2017 Phys. Rev. B 95 134409
[64] Zhang S and Li Z 2004 Phys. Rev. Lett. 93 127204
[65] MicroMagnum—Fast Micromagnetic Simulator for computations on CPU and GPU micromagnum.informatik.uni-hamburg.de
[66] Vansteenkiste A, Leliaert J, Dvornik M, Helsen M, Garcia-Sanchez F and Van Waeyenberge B 2014 AIP Adv. 4 0–22
[67] Camosi L et al 2017 Phys. Rev. B 95 214422
[68] Hoffmann M, Zimmermann B, Müller G P, Schürhoff D, Kiselev N S, Melcher C and Blügel S 2017 arXiv:1702.07573
[69] Kosevich A, Ivanov B and Kovalev A 1990 Phys. Rep. 194 117–238
[70] Thiaville A, Rohart S, Jué É, Cros V and Fert A 2012 Europhys. Lett. 100 57002
[71] Dupé B, Kruse C N, Dornheim T and Heinze S 2016 New J. Phys. 18 055015
[72] Hobart R H 1963 Proc. Phys. Soc. 82 201–3
[73] Derrick G H 1964 J. Math. Phys. 5 1252–4
[74] Sampaio J, Cros V, Rohart S, Thiaville A and Fert A 2013 Nat. Nanotechnol. 8 839–44
[75] Rohart S, Miltat J and Thiaville A 2016 Phys. Rev. B 93 214412